Solid State Phenomena
ISSN: 1662-9779, Vol. 388, pp 11-19
doi:10.4028/p-y1W1Ey

Submitted: 2025-12-09
Revised: 2026-02-09
Accepted: 2026-02-19
Online: 2026-04-15

Work Hardening of Dual Phase Steel in Subsequent Tensile Testing with Post-Necking Large Pre-Strain

Takashi Matsuno[1,a*], Keisuke Hokimoto[1,b], Kazuyuki Shimizu[1,c], Takayuki Hama[2,d] and Yoshiaki Honda[3,e]

[1]Faculty of Engineering, Tottori University, 4-101 Koyama-cho-minami, Tottori, Tottori 680-8552, Japan

[2]Graduate School of Energy Science, Kyoto University, Yoshida-Honmachi, Sakyo-ku, Kyoto 606-8501, Japan

[3]Nippon Steel Corporation, 20-1 Shintomi, Futtsu-City, Chiba, 293-8511 Japan

[a*]matsu@tottori-u.ac.jp, [b]M24J3049X@edu.tottori-u.ac.jp, [c]ksmz@tottori-u.ac.jp, [d]hama.takayuki.4s@kyoto-u.ac.jp, [e]honda.x66.yoshiaki@jp.nipponsteel.com

Keywords: tensile test, strain-aging, pre-strain, post-necking, dual phase steel.

Abstract. For high-accuracy finite element (FE) simulation of automobile crashing behavior, a work hardening curve that involves pre-strain from press forming is required. Here, the plastic strains exceeding the uniform deformation region are generally introduced through processes such as bending, but such large pre-strain effect have not been reported. Therefore, in this study, for DP590 steel, the work hardening curve for second-stage tension under pre-strain exceeding the uniform deformation region was identified. This identification was enabled by the diameter measurement tensile test developed by the authors. As a result, in the second-stage tension in the same direction as the first-stage tension, the initial yield stress showed a tendency to overshoot relative to the original work hardening curve, revealing that strain aging occurred. The overshoot portion formed a stress plateau that continued up to an equivalent plastic strain of 0.18. Such a tendency has not been observed in DP590 steel, making this a phenomenon revealed for the first time. When the tensile direction in the second stage was orthogonal to the first stage, the cross-hardening effect (reduction in initial yielding due to the Bauschinger effect and overshoot from the original work hardening curve) was observed. The stress plateau region due to overshoot continued up to an equivalent plastic strain as large as 0.6. These large plateaus concluded that work hardening presents perfect plasticity at large deformed press parts.

Introduction

To achieve both weight reduction and crashworthiness in automobiles, advanced high-strength steel (AHSS) sheets have become widely adopted. As material strength increases, equivalent crushing performance can be obtained even with reduced sheet thickness. Although problems specific to AHSS exist, such as tool damage [1], delayed fracture [2] caused by remarkably high tensile residual stress [3, 4] combined with deformation-induced microstructural changes [5, 6], and incidental fracture during press forming [7], significant progress has been made in addressing these issues in recent years. Indeed, automobile frames incorporating materials with more than 60% AHSS content have been released.

For the design of crash components, crash simulations using the finite element method (FEM) are often performed in advance. FEM requires input of the work-hardening curve of the material used in the frame. The work-hardening curve of as-received material is often employed as input. However, to improve the accuracy of crash FEM, a work-hardening curve that accounts for plastic strain during press forming is necessary.

The simplest approach involves directly subtracting the plastic strain imposed by press forming from the work-hardening curve of as-received material. However, deformation during crash involves path changes relative to deformation during press forming. When the deformation path changes, a decrease in yield stress due to the Bauschinger effect occurs, followed by an overshoot from the original work-

hardening curve [8–10]. These behaviors are collectively termed the cross-hardening effect, and their characteristics have been analyzed through various experiments [8–10].

In most cases investigating the cross-hardening effect, plastic deformation prior to strain path change remains below uniform elongation. This is because specimens extracted from necked test pieces do not exhibit uniform elongation, and conventional tensile tests cannot measure the work-hardening curve beyond this point. However, pre-strain levels below uniform elongation are not necessarily sufficient for practical applications. Because AHSS exhibits relatively low ductility, press forming is performed primarily through bending deformation. During bending processes, plastic strains exceeding uniform elongation are commonly encountered.

Therefore, in this study, identification of the work-hardening curve was attempted for 590 MPa class dual-phase (DP) steel subjected to a 90-degree deformation path change. At ESAFORM 2024, the authors reported the relationship between true stress (σ_t) and cross-sectional area reduction (ρ) obtained using diameter-measurement-type tensile testing [11], which was developed by the authors [12–14]. The present work identifies the flow stress curve through FE simulation based on the σ_t–ρ curve measured in the previous study.

Experimental and Simulation Methods

Material

A DP steel with a tensile strength of 560 MPa was used as the test material. Its chemical component and mechanical properties are shown in **Tables 1** and **2**, respectively. The steel was fabricated in the laboratory with the intention of being equivalent to DP590.

Table 1. Chemical components of tested steel (mass%).

C	Si	Mn
0.038	0.50	1.50

Table 2. Mechanical properties of tested steel.

Yield stress [MPa]	Tensile strength [MPa]	Uniform elongation [%]	Total elongation [%]
335	561	19	31

Preparing small round-bar specimen

The compact round bar tensile test with pre-strain introduction has already been reported at ESAFORM 2024 [11] and is described again below.

No. 5 type specimens with 2.5-mm thickness, standardized by Japanese Industrial Standards (JIS) Z2241, were subjected to preliminary tensile testing before subsequent compact tensile tests. Hereafter, this sheet-type tensile testing is referred to as JIS5 tensile test. The JIS5 specimens were elongated up to 23% under post-necking conditions. To estimate the local Mises strain, measurement by digital image correlation (ARAMIS system, GOM) was performed in advance on one JIS5 tensile test. The distribution of Mises strain is shown in **Fig. 1**, with a maximum value of approximately 0.31.

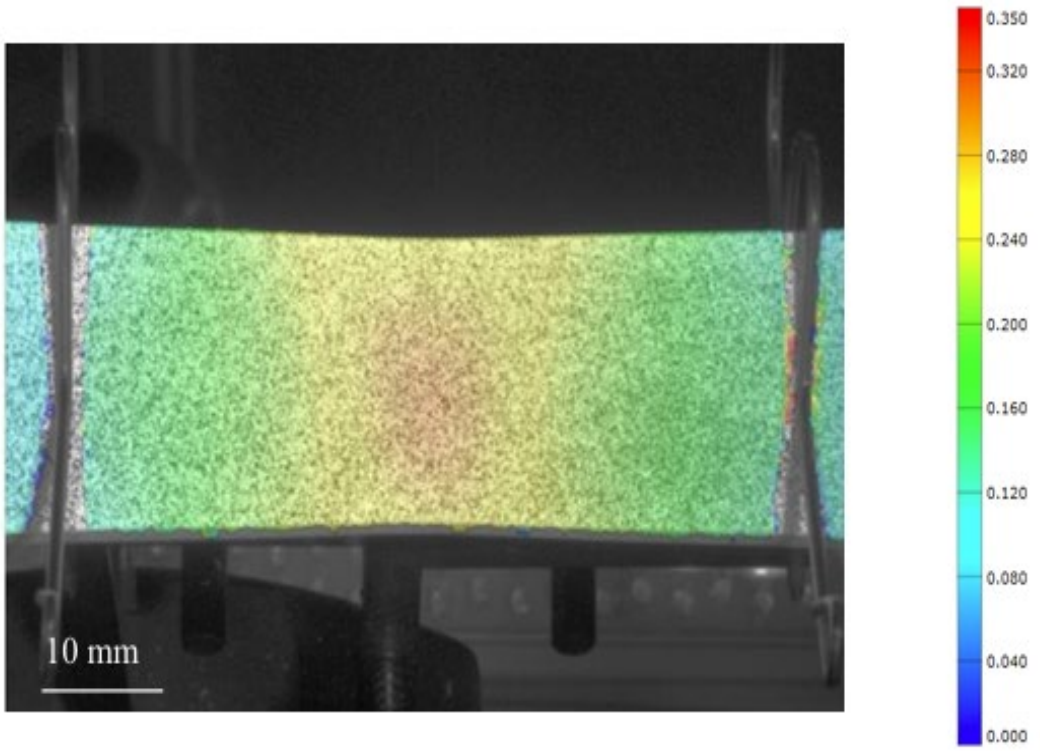

Fig. 1. Equivalent (Mises) strain distribution in JIS5 tensile test at 23% elongation.

As depicted in **Fig. 2**, the preliminary tensile test was aligned such that the tensile direction of the small round-bar specimens corresponded to the transverse direction of the cold-rolling process (referred to as the transverse direction). Accordingly, the JIS 5 specimens were elongated in the transverse direction, and subsequent tensile specimens were extracted in two orientations: one aligned with the transverse direction, representing no strain path change (**Fig. 2a**), and the other aligned with the rolling direction, such that the subsequent tensile direction was perpendicular to the preliminary tensile direction (**Fig. 2b**). It should be noted that this configuration does not constitute a strictly orthogonal strain path change in a rigorous sense, because diffuse necking developed in the JIS 5 specimens (as shown in **Fig. 1**), resulting in a stress state that deviated from pure uniaxial tension prior to the extraction of the subsequent specimens.

With such large pre-strain, virtually no uniform elongation is observed in the subsequent tensile testing. Consequently, work-hardening curves cannot be identified using conventional sheet-type tensile specimens with elongation measurement. The compact tensile testing system with real-time diameter measurement developed by the authors enables the determination of the true stress versus true strain curve in the post-necking region by measuring the diameter at the necking section instead of elongation. As described later, work-hardening curves can be identified through FEM-based curve fitting using the measured load and diameter values as references. Although it may be suggested that measuring the rectangular cross-sectional area of sheet-type specimens would suffice, unlike circular cross-sections, the rectangular shape is not maintained in the post-necking region, making accurate measurement of the cross-sectional geometry difficult.

The design of the small round-bar specimens is presented in **Fig. 3**. The thinnest part of these specimens had a diameter of 1.0 mm, enabling their extraction from the JIS 5 specimens that had undergone pre-straining exceeding the onset of necking.

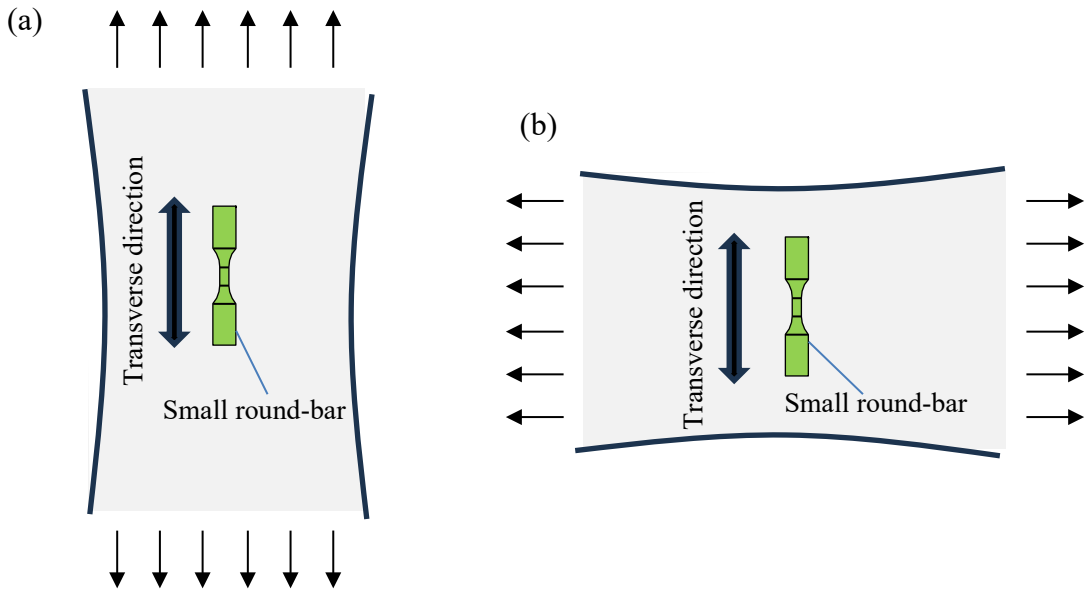

Fig. 2. Sampling position of the small round-bar specimens and the tensile direction of the JIS 5 tensile test prior to compact tensile testing: (a) subsequent tensile direction parallel to the preliminary tensile direction (FD case) and (b) subsequent tensile direction perpendicular to the preliminary tensile direction (OD case).

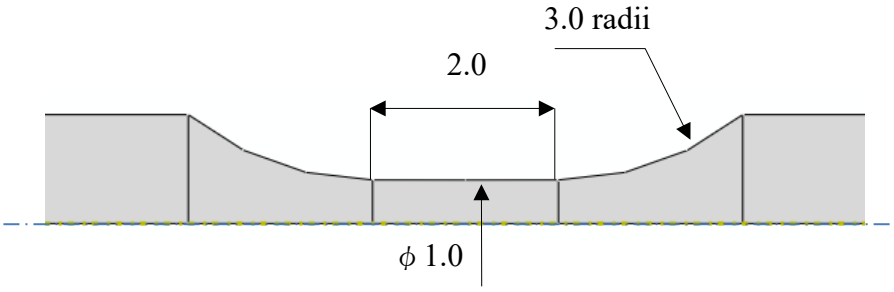

Fig. 3. Geometry of the small round-bar specimen depicted in an axisymmetric two-dimensional drawing.

Compact tensile test with real-time diameter measurements

After extracting the small round-bar specimens, compact tensile tests with real-time diameter measurements were executed, generating $\sigma_t - \rho$ curves. In these compact tensile tests, the diameters, D_a and D_b, of the thinnest cross-sectional area under tension were continuously measured in two directions. The diameter measurements were performed using an LED-projection-type dimension measuring instrument (Keyence TMX 5006). Although the dimensional measurement accuracy is ±0.2 μm, the measured values contain scatter due to the algorithm used to identify the minimum diameter section. Further details can be found in the authors' previous work [14]. The specimen was oriented such that D_b corresponded to the thickness of the original steel material. The σ_t and ρ in the cross-section were calculated as follows:

$$\sigma_t = \frac{4F}{\pi D_a D_b}, \tag{1}$$

$$\rho = \ln\left(\frac{D_0^2}{D_a D_b}\right), \tag{2}$$

where D_0 corresponds to the initial diameter of the specimen (1.0 mm).

FE Simulation

Furthermore, to reproduce the measured $\sigma_t - \rho$ curve, the flow stress curve was identified through tensile simulations using FEM. A two-dimensional axisymmetric model was employed, and conventional boundary conditions were applied, in which one end was fixed and the other was driven under displacement control. Further details can be found in our previous publications [12, 13, 15]. The commercial static implicit FEM solver Abaqus Standard was used for the computation. Even for materials that exhibit upper yield point in elongation-measurement-type tensile tests, they do not show it in geometry-measurement-type tensile tests. Therefore, based on the original work hardening curve offset by the amount of pre-strain (equivalent strain), a flow stress curve composed of three parts was assumed: the yield stress reduction part corresponding to the Bauschinger effect (**Eq. (3)**), the yield stress overshoot and plateau part (**Eq. (4)**), and the return to the original curve. These parts transition at specific strain values $\overline{\varepsilon}_B$ and $\overline{\varepsilon}_S$. In addition, in the latter part of the work hardening curve, a linear term K_l was multiplied as shown in **Eq. (5)** to correct the deviation from the reference curve $Y_{shift}(\overline{\varepsilon}_p)$.

$$Y_{st}(\overline{\varepsilon}_p) = \kappa(\overline{\varepsilon}_p + \gamma)^{\eta} \qquad \text{for } \overline{\varepsilon}_p < \overline{\varepsilon}_B \tag{3}$$

$$Y_{st}(\overline{\varepsilon}_p) = Y_{const} \qquad \text{for } \overline{\varepsilon}_B \leq \overline{\varepsilon}_p < \overline{\varepsilon}_S \tag{4}$$

$$Y_{st}(\overline{\varepsilon}_p) = K_l Y_{shift}(\overline{\varepsilon}_p) \qquad \text{for } \overline{\varepsilon}_p \geq \overline{\varepsilon}_S\,. \tag{5}$$

$Y_{shift}(\overline{\varepsilon}_p)$ is the offset curve of the original (without pre-straining) flow stress curve $Y(\overline{\varepsilon}_p)$, expressed as

$$Y_{shift}(\overline{\varepsilon}_p) = Y(\overline{\varepsilon}_p + \overline{\varepsilon}_{pre}) \tag{6}$$

where $\overline{\varepsilon}_{pre}$ is the pre-strain.

The original (without pre-straining) flow stress curve $Y(\overline{\varepsilon}_p)$ was identified using small round-bar tensile specimen with integration of real time diameter measurement and FE simulation. The curve is identified as:

$$Y(\overline{\varepsilon}_p) = (1-a)Y_1(\overline{\varepsilon}_p) + a(Y_2(\overline{\varepsilon}_p) + \mathrm{b}) \tag{7}$$

where $Y_i(\overline{\varepsilon}_p)$, $i = 1, 2$, denotes Swift work-hardening law as follows:

$$Y_i(\overline{\varepsilon}_p) = K_i(\overline{\varepsilon}_p + c_i)^{n_i}. \tag{8}$$

a and b are the parameters for switching from $Y_1(\overline{\varepsilon}_p)$ to $Y_2(\overline{\varepsilon}_p)$ in $Y(\overline{\varepsilon}_p)$ as

$$a = \frac{\tanh\left(50(\overline{\varepsilon}_p - \overline{\varepsilon}_{switch})\right)+1}{2} \tag{9}$$

$$b = Y_2(\overline{\varepsilon}_{switch}) - Y_1(\overline{\varepsilon}_{switch}). \tag{10}$$

Here, $\overline{\varepsilon}_{switch}$ represents the plastic strain corresponding to the transition from $Y_1(\overline{\varepsilon}_p)$ to $Y_2(\overline{\varepsilon}_p)$. The identified parameters are shown in **Table 3**.

Table 3 Parameters of the $Y(\overline{\varepsilon}_p)$ identified through compact tensile testing combined with FE simulation.

K_1	n_1	c_1	K_2	n_2	c_2	$\overline{\varepsilon}_{switch}$
882.0	0.152	0.00165	809.7	0.11	0.00031	0.20

Results and Discussion

Figure 4 presents the flow stress curves identified through subsequent compact tensile testing integrated with FE simulation. The identified parameters are listed in **Table 4**. The flow stress curves in **Fig. 4** are normalized by the respective K_l values, such that the curves coincide in the larger strain region ($\overline{\varepsilon}_p \geq \overline{\varepsilon}_S$) under all conditions.

First, in the following direction (FD)—where the JIS 5 and subsequent tensile testing directions are identical—the flow behavior in the small strain region is characterized by an overshoot followed by a stress plateau. The initial yield stress is approximately 40 MPa higher than $Y_{shift}(0)$. (Because this value is normalized by K_l, it does not necessarily correspond to Y_{const} in **Table 4**). The results indicate that this stress plateau persists until $\overline{\varepsilon}_p = 0.18$.

In contrast, during tension in the orthogonal direction (OD), the initial yield stress decreases by approximately 80 MPa, indicating a clear Bauschinger effect. The flow stress then increases to 810 MPa before forming a stress plateau. This plateau persists up to $\overline{\varepsilon}_p = 0.60$, a behavior consistent with nearly perfect plasticity.

Figure 5 provides a comparison between the measured and FE-simulated $\sigma_t - \rho$ curves. Although the shape differs considerably from the work-hardening curves in **Fig. 4**, this is attributable to the hydrostatic stress arising from necking. In the strain range corresponding to the stress plateau region, the true stress increases due to the development of hydrostatic stress caused by necking [15]. Since the equivalent stress under the von Mises yield criterion does not include the hydrostatic stress component, the equivalent stress itself does not increase even when the hydrostatic stress becomes large due to necking, that is, even when the true stress increases. Consequently, the true stress continues to increase even when the work-hardening curve exhibits a plateau. The increase in hydrostatic stress due to necking is widely recognized through the Bridgeman analysis[16]. With this understanding, examination of **Fig. 5** confirms that the FE simulation, which utilizes the flow stress curves from **Fig. 4**, accurately reproduces the measured values. **Fig. 5a** also displays a linear fit line in the small strain region, revealing that σ_t deviates from this tangent at approximately $\rho = 0.18$. This observation corroborates the finding that the stress plateau region persists until $\overline{\varepsilon}_p = 0.18$. In the plateau region of the flow stress curve, the hydrostatic stress generated by necking produces a slight gradient in the $\sigma_t - \rho$ curve as described above.

In the case of OD tension (**Fig. 5b**), the measured data exhibit a plateau region even on the $\sigma_t - \rho$ curve. Considering the slight gradient of σ_t observed in FD tension (**Fig. 5a**), such a plateau implies a gradual decrease in flow stress. Actually, from approximately $\rho = 0.20$ onward, the σ_t predicted by the FE simulation is slightly higher than the measured values. This discrepancy suggests that incorporating work softening into the flow stress curve could improve the agreement; however, introducing work softening into the FE simulation severely deteriorates numerical convergence, and resolving this discrepancy was not achieved in the present study. Nevertheless, this discrepancy is not substantial, and the existence of an extended plateau over a remarkably large range of plastic strain, or a gradual work softening trend, is an unambiguous observation from the experimental results. Given that the use of a work softening curve must be avoided due to the convergence difficulty, the nearly perfectly plastic flow stress curve derived in Fig. 4 represents a reasonable approximation for predicting the actual deformation behavior.

It is noteworthy that such differences are observed between the FD and OD cases despite both exhibiting stress plateaus. The detailed mechanism underlying this difference remains unclear at this stage. We hypothesize that the plateau region inherently exhibits a slight softening tendency, which becomes more apparent in the $\sigma_t - \rho$ curve for cases with a wider plateau region, such as the OD case. This hypothesis requires detailed verification based on micromechanics, which we intend to pursue through inverse deformation analysis [17, 18].

The increase in initial yield stress during FD tension is a behavior not previously observed for this DP590 steel. A significant time-lapse of approximately two months occurred between the initial JIS 5 tensile test and the subsequent small round bar test. Consequently, there is a high probability that

static strain aging occurred during this period. It is possible that strain aging also affected the material response in the OD case.

These results suggest that components containing regions of large deformation, such as bent sections, may exhibit higher-than-anticipated strength. This strength exceeds predictions based on the original flow stress curve obtained from a conventional JIS 5 tensile specimen.

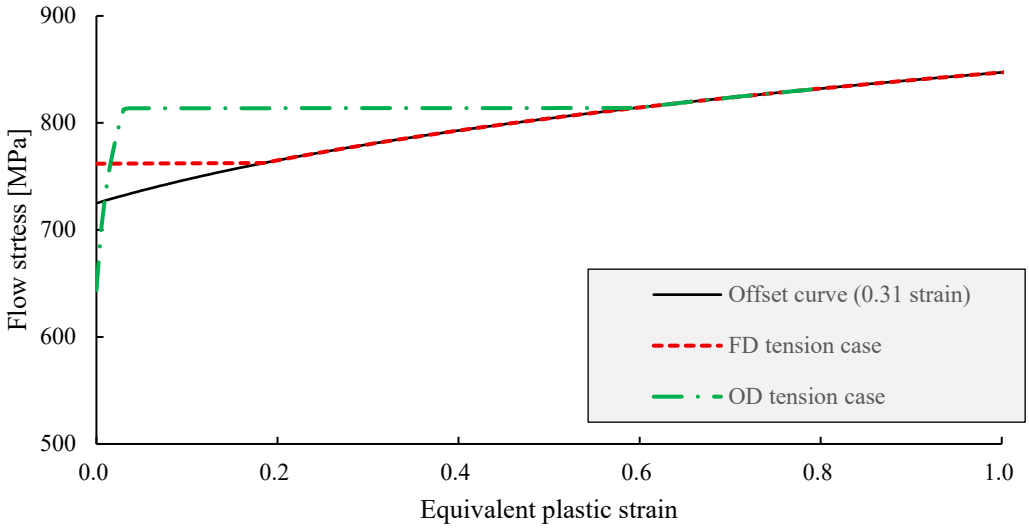

Fig. 4 Identified flow stress curves.

Table 4. Parameters for $Y_{st}(\bar{\varepsilon}_p)$ identified by subsequent compact tensile testing (following the JIS 5 tensile test) combined with FE simulation.

Direction relative to JIS 5	$\bar{\varepsilon}_{pre}$	κ	γ	η	Y_{const}	$\bar{\varepsilon}_B$	$\bar{\varepsilon}_S$	K_l
Same	0.31	-	-	-	800	-	0.145	1.06
Orthogonal	0.31	1229.8	0.12	0.0051	821	0.030	0.595	1.01

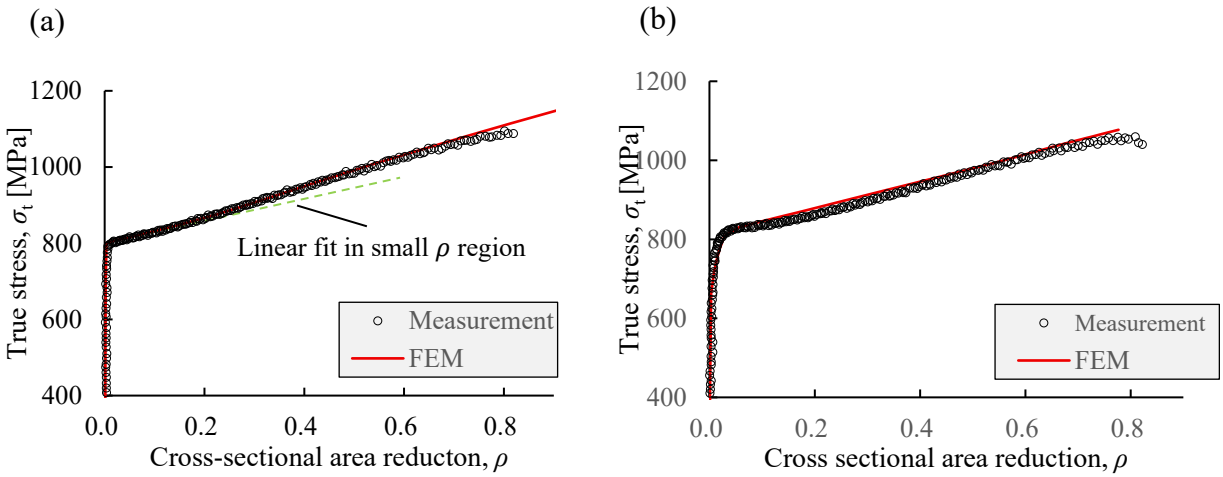

Fig. 5. σ_t–ρ curves of measurement and FE simulation: (a) FD and (b) OD tensile tests.

Summary

This study investigated the influence of strain path changes on the work hardening behavior of DP590 AHSS following post-necking tensile deformation.

In the experiment procedure, sheet specimens were first subjected to tensile deformation until necking occurred. Small round-bar tensile specimens were then extracted from the necked region. The flow stress curve for this second-stage tensile test (on the small round-bars) was identified by ensuring that an FE simulation accurately reproduced the measured diameter change and true stress. The key findings are as follows:

1) When the material was subjected to large pre-deformation, an increase in the initial yield stress of the subsequent tensile test was observed, even without a change in the tensile direction. This behavior is presumably attributable to strain aging, although further investigation is required to confirm this mechanism.
2) When the second-stage tensile direction was perpendicular to the preliminary tensile direction, the identified flow stress curve exhibited a nearly flat plateau, suggesting behavior approaching perfect plasticity. It should be noted, however, that the agreement between the experimental and simulated results for the OD case (**Fig. 5b**) is less satisfactory than that for the FD case (**Fig. 5a**), and the identified flow stress curve for the OD case should therefore be regarded as preliminary.

This finding suggests that components containing regions of large deformation (such as bent sections) that have experienced post-necking strains may exhibit higher structural strength than would be predicted by the original flow stress curve.

References

[1] T. Matsuno, K. Nakagiri, T. Matsuda, T. Tanaka, T. Yasutomi, H. Shoji, & M. Ohata, Identification of ductile fracture design curve for hardened quasi-brittle AISI-D2 tool steel to predict shearing tool failure, J. Mater. Process. Technol., 307(2022), 117680. https://doi.org/10.1016/j.jmatprotec.2022.117680.

[2] T. Matsuno, Y. Ueda, T. Takahashi, T. Hama, T. Hojo, Y. Shibayama, M. Ridha, Y. Okitsu, & M. Takamura, Delayed fracture stress thresholds degraded by shear punching process in ultra-high-strength steel sheets: Analysis using an in-plane bending test with numerical assimilation, J. Manuf. Process., 119 (2024) 1005-1021. https://doi.org/10.1016/j.jmapro.2024.04.013.

[3] J. Eguchi, T. Matsuno, Y. Kunii, K. Shimizu, Y. Matsuki, T. Shinmiya, & E. Iizuka, Observation-driven punching simulation using a quasi-nonparametric ductile fracture locus, J. Mater. Process. Technol., (2026) 119243. https://doi.org/10.1016/j.jmatprotec.2026.119243.

[4] T. Matsuno, Y. Ochiai, Y. Okitsu, M. Iga, A. Khori, & T. Mikami, Surface and interior residual stress analysis of a deep-drawn 1180 MPa class ultra-high strength steel sheet with scratch marks, Int. J. Adv. Manuf. Technol., 116 (2021) 2873-2884. https://doi.org/10.1007/s00170-021-07675-2.

[5] T. Matsuno, N. Kinoshita, T. Matsuda, Y. Honda, & T. Yasutomi, Microvoid formation of ferrite-martensite dual-phase steel via tensile deformation after severe plastic shear-deformation, ISIJ Int., 63 (2023) 941-949. https://doi.org/10.2355/isijinternational.ISIJINT-2023-012.

[6] T. Matsuno, Y. Sekito, & K. Kawasaki, Microstructure characterization of fine grains near hot-sheared surface formed during hot-stamping process, J. Mater. Process. Technol., 229 (2016) 570-581. https://doi.org/10.1016/j.jmatprotec.2015.10.012.

[7] T. Matsuno, N. Kinoshita, K. Shimizu, H. Shoji, & M. Ohata, Microstructural feature-driven post-mortem analysis of plastic strain and stress triaxiality in ductile-fractured ferrite-martensite dual-phase steel: Integrating microstructural observations and mesoscale finite element simulations, J. Mater. Res. Technol. 39(2025), 3087-3102. https://doi.org/10.1016/j.jmrt.2025.09.265.

[8] M. Joo, M. S. Wi, S. Y. Yoon, S. Y. Lee, F. Barlat, C. N. Tome, B. Jeon, & Y. Jeong, A crystal plasticity finite element analysis on the effect of prestrain on springback, *Int. J. Mech. Sci.*, 237(2023), 107796. https://doi.org/10.1016/j.ijmecsci.2022.107796.

[9] J. Liao, J. A. Sousa, A. B. Lopes, X. Xue, F. Barlat, & A. B. Pereira, Mechanical, microstructural behaviour and modelling of dual phase steels under complex deformation paths, *Int. J. Plasticity*, 93(2017), 269-290. https://doi.org/10.1016/j.ijplas.2016.03.010.

[10] F. Barlat, G. Vincze, J. J. Grácio, M. G. Lee, E. F. Rauch, & C. N. Tomé, Enhancements of homogenous anisotropic hardening model and application to mild and dual-phase steels, *Int. J. Plasticity*, 58(2014), 201-218. https://doi.org/10.1016/j.ijplas.2013.11.002.

[11] T. Matsuno, N. Kinoshita, K. Hokimoto, T. Hama, & Y. Honda, Enhancement of fracture strain during abrupt orthogonal strain-path changes in ferrite/martensite dual phase steel, *Mater. Res. Proc.*, 41(2023), 118. https://doi.org/10.21741/9781644903131-118.

[12] T. Matsuno, D. Kondo, T. Hama, T. Naito, Y. Okitsu, S. Hayashi, K. Takada, Flow stress curves for 980MPa- and 1.5GPa-class ultra-high-strength steel sheets weakened under high-stress triaxiality, Int. J. Mech. Sci., 261(2024), 108671. https://doi.org/10.1016/j.ijmecsci.2023.108671.

[13] T. Matsuno, T. Fujita, T. Matsuda, T. Shibayama, T. Hojo, I. Watanabe, Unstable stress-triaxiality development and contrasting weakening in two types of high-strength transformation-induced plasticity (TRIP) steels: Insights from a new compact tensile testing method, J. Mater. Process. Technol., 322(2023), 118174. https://doi.org/10.1016/j.jmatprotec.2023.118174.

[14] T. Matsuno, Y. Yamazaki, S. Matsubara, J. Eguchi, K. Shimizu, M. Koyama, ... & T. Tsuchiyama, Local work-hardening and Lüders deformation invariance in TRIP-aided medium-Mn high-strength steel: Significant TRIP effect changes in the warm temperature range up to 200°C, *J. Jpn. Soc. Technol. Plast.*, 66(2025), 61-68. https://doi.org/10.9773/sosei.240702.

[15] T. Matsuno, K. Furukawa, Y. Okitsu, M. Koyama, & T. Tsuchiyama, Local yield stress and its unusual independence on multi-axial stress states during Lüders deformation of medium-Mn, high-strength steel, ISIJ Int., 64 (2024) 859-867. https://doi.org/10.2355/isijinternational.ISIJINT-2023-326.

[16] P.W. Bridgman, Studies in Large Plastic Flow and Fracture, McGraw-Hill, New York, 1952.

[17] T. Matsuno, N. Okumura, Y. Fukuda, K. Shimizu & T. Murai, Direct solution of inverse deformation problem for dual-phase steel microstructures: U-net deep fake for pseudo-inverse finite-element simulation using representative volume elements, Mater. Today Commun., 46(2025), 112769. https://doi.org/10.1016/j.mtcomm.2025.112769.

[18] T. Matsuno, Y. Fukuda, K. Shimizu, H. Shoji, M. Ohata, N. Yamashita, H. Yokota & T. Murai, Image-assimilation of deformed dual-phase steel microstructure via U-net deep learning, Mater. Res. Proc., 54(2025), 963-970. https://doi.org/10.21741/9781644903599-103.